

Article

The PT/S-Box of Modular Cellulase AcCel12B Plays a Key Role in the Hydrolysis of Insoluble Cellulose

Yuwei Li ^{1,2}, Junling Wang ^{1,3}, Limei Wang ¹, Hao Tong ¹, Mingwei Bu ¹, Gui Gao ¹, Weiwei Han ¹ and Zuoming Zhang ^{1,*} 

¹ Key Laboratory for Molecular Enzymology & Engineering of the Ministry of Education, School of Life Science, Jilin University, Changchun 130012, China; ywli14@mails.jlu.edu.cn (Y.L.); wangjl09@mails.jlu.edu.cn (J.W.); wanglm16@mails.jlu.edu.cn (L.W.); tonghao16@mails.jlu.edu.cn (H.T.); bumw15@mails.jlu.edu.cn (M.B.); gaogui@jlu.edu.cn (G.G.); weiweihan@jlu.edu.cn (W.H.)

² State Key Laboratory of Supramolecular Structure and Materials, College of Chemistry, Jilin University, Changchun 130012, China

³ Department of Bioengineering, Jilin Agricultural Science and Technology University, Jilin 132101, China

* Correspondence: zmzhang@jlu.edu.cn; Tel.: +86-431-8515-5218

Received: 24 February 2018; Accepted: 11 March 2018; Published: 20 March 2018

Abstract: Cellulases play key roles in the degradation of lignocellulosic materials. The function and mechanism of the catalytic domain (CD) and carbohydrate-binding module (CBM) of cellulases were earlier revealed by analysis and characterization of protein structure. However, understanding of the catalytic mechanism of the entire enzyme, and the analysis of the catalytic model, were inadequate. Therefore, the linker chain between CD and CBM has been extensively studied to bridge this gap. Cellulase AcCel12B and three mutants with different linker lengths (with no or 1–3 PT/S-box units) were successfully constructed and purified. Results showed that the activity of cellulases on Avicel and regenerated amorphous cellulose (RAC) increased with the number of PT/S-box units. Furthermore, the desorption of AcCel12B and its mutants from RAC and Avicel were significantly different. The energy of desorption of wild-type and mutant AcCel12B from cellulose decreased with the number of PT/S-box units. Thus, AcCel12B containing more PT/S-box units was more easily desorbed and had more opportunity to hydrolyze cellulose than other samples. The number of PT/S-box units in endocellulase affected the desorption of the enzyme, which is possibly responsible for the differences in the activity of wild-type and mutant AcCel12B on Avicel and RAC.

Keywords: cellulase; linker; cellulose; PT/S-Box

1. Introduction

Cellulose, the most abundant natural homopolymer of D-glucose units linked by β -1,4-glycosidic bonds, differs from other polysaccharides in terms of solubility, structural rigidity, and resistance to biological disintegration [1]. Cellulases can hydrolyze β -1,4-glycosidic bonds of cellulose to produce oligomeric cellulose or cellooligosaccharides. Enzymatic hydrolysis of cellulose is a complex process that is accomplished by the synergistic action of at least three types of cellulases [2,3]. Most cellulases are typical modular enzymes that consist of one or two catalytic domains (CD), one or several carbohydrate-binding modules (CBM), and other modules of unknown function, which are separated by a distinct linker region (LR) [4]. The CBM adsorbed on the cellulose surface targets the CDs to the insoluble substrate and increases the local concentration of cellulases. Next, the CD cleaves the cellulose chains on the regions of low crystallinity to yield oligosaccharides and/or cellobiose [5]. The linker performs various functions, such as providing cold adaptation to cellulase of an Antarctic bacterium [4], separating the CD and CBM by a necessary distance, facilitating the dynamic adsorption of CBM on the substrate [6], acting as a molecular spring between two functional modules [6], and affecting

the affinity of cellulase for lignin and cellulose [7]. Kont et al. recently reported that the synergism between the CBM-linker and CD plays an important role in movement of the cellulose chain into the active site of the processive endoglucanase Cel7A from *Trichoderma reesei* [8]. However, understanding the functions and molecular mechanisms of the linker has been challenging, as it belongs to the class of intrinsically disordered proteins (IDPs), and the length and sequence of the linker showed low conservation [9].

Whole or partial sequences of certain linkers showed similarities in terms of content enrichment of proline, threonine and serine, which were often repeated in the LR as a Pro-Thr/Ser box (PT/S-box) [10,11]. The PT-box is ubiquitous in many modular glycoside hydrolases and its number of amino acids is indefinite. For example, the xylanase Cex from *Cellulomonas fimi* contains a short PS-box [12]. The mannanase from *Caldibacillus cellulovorans* contains PS-boxes of three different lengths [13]. The endocellulase Cel5A from *Acidothermus cellulolyticus* 11B had a PT-box of approximately 40 amino acids, whereas the endoglucanase (GuxA) of GH12 from the same strain contained PS-boxes of three different lengths [14]. It is widely accepted that the PT-box plays an important role in protein solubility and catalytic activity of cellulase [11,15]. Small-angle X-ray scattering (SAXS) and nuclear magnetic resonance (NMR) spectroscopic results indicate that in solution, the PT-box does not have any significant structure or stable conformation, but exhibits an extended, knotted and rigid conformation [16,17]. Poon et al. demonstrated that the PT-box linker is a flexible tether that provided flexibility to the catalytic domain for hydrolyzing neighboring xylan chains [12]. Furthermore, the threonine and serine of fungal cellulases are normally glycosylated [18] and thus favor more extended conformations [19] when dynamically combined with crystalline cellulose, as indicated by molecular dynamics (MD) simulations [20]. Therefore, the PT-box of cellulases may interact with the solid substrate (cellulose) when the enzymes hydrolyze cellulose. However, the molecular mechanisms underlying PT-box catalysis and the interactions between the PT-box and the substrate are not known. Further, since the lengths of PT-boxes vary considerably, it is difficult to define a PT-box unit.

The endocellulase AcCel12B from thermophilic bacterium *A. cellulolyticus* 11B is composed of a CD and CBM separated by a flexible 48-amino-acid-long LR [21]. The LR of AcCel12B comprises a PT/S-box and two unconserved regions that connect the CD and CBM. Interestingly, the PT/S-box was separated into two parts by a glycine, and the amino acid sequences of the two parts were axisymmetrically arranged with glycine as the axis of symmetry. To evaluate the function of the PT/S-box in cellulose hydrolysis, we defined each part of PT/S-box as one PT/S-box unit and then redesigned the numbers of PT/S-box units in the linker. The catalytic activities of the wild-type and LR mutant AcCel12B towards different substrates and the catalytic processes were evaluated. The adsorption and desorption of the wild-type and mutant enzymes with different substrates were also determined. Experimental measurements showed that the number of PT/S-box units affected enzyme activity and desorption of enzyme from solid substrate.

2. Results and Discussion

2.1. Mutant Design of AcCel12B Linker

The LR of AcCel12B contains 48 amino acids, as predicted by homology modeling analysis (Figure 1). The amino acid sequence of the LR consists of alternating prolines and threonines (serines) (PT/S-box) located in the middle of the LR and two irregular sequences that connect the CD and CBM. The PT/S-box of AcCel12B is separated into two regions by a glycine. The amino acid sequence of each region is $(PT)_2(PS)_4P$ (PT-box1) and $(PS)_4(PT)_2S_2P$ (PT-box2) (Figure 1). Therefore, PT-box1 and PT-box2 were axisymmetrically arranged by the glycine. The backbone conformation of proline was restricted because of the bulkiness of the N-CH₂ side-chain group [22]. Since the amide proton of proline was replaced by a CH₂ group, it was unable to act as a hydrogen bond donor [23]. In contrast, the hydroxyl groups of serine and threonine that precede proline form a regular order and act as hydrogen bond donors [24]. In addition, the hydroxyl groups of the sugar chains are also arranged

outwardly in a regular order on the 110 surfaces of microcrystalline cellulose [25], allowing hydrogen bonds to be formed between these surfaces and the T or S of the PT/S-boxes. Alanine is highly flexible, which increases the flexibility of the polypeptide chain [26,27]. Thus, alanine may act as a hinge that renders semi-flexibility to the otherwise-stiff PT/S-box polypeptide chain. Reports show that linker length and stiffness play a critical role in the cooperative action of cellulase domains [28]. The hinge bending motion of the semi-stiff linker is beneficial for the synergistic effect of the cellulase domains [28,29]. However, quantification of the relationship between linker length and stiffness of the PT-box is challenging. The PT/S-box is composed of two axisymmetric regions of similar length in the case of AcCel12B. Other sources of PT-boxes, such as Cel5A and GuxA from *A. cellulolyticus* 11B [14] and mannanase from *C. cellulovorans* [13], are also separated into two or several axisymmetric regions by alanines or other amino acids; however, the length of each region is different. Hence, we defined the PT-box1, (PT)₂(PS)₄P, as one PT/S-box unit and then redesigned the LR of AcCel12B to contain 0, 1, 2 and 3 PT/S-box units (Figure 1).

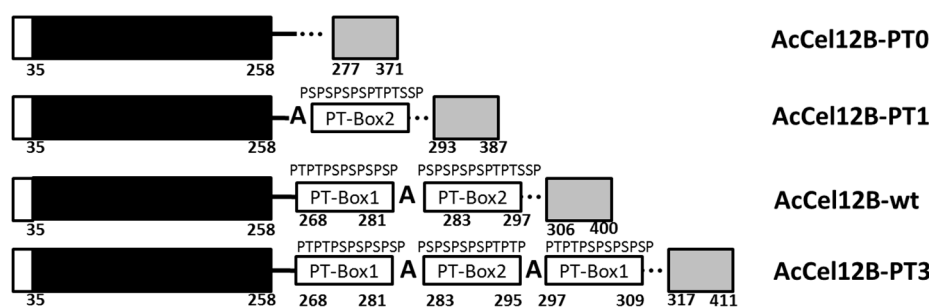


Figure 1. Schematic representation of the structures of wild-type and mutant AcCel12B. Structures of native full-length thermophilic cellulase, AcCel12B (the numbering corresponds to the amino acid sequence of the mature protein), and its mutants, AcCel12B-PT0, AcCel12B-PT1, and AcCel12B-PT3. The signal peptides are represented by the open boxes, the CDs by black boxes, the LRs by continuous line, and the CBMs by gray boxes. The rectangles on the LR correspond to the PT/S-Box. PT: Proline-Threonine. PS: Proline-Serine. CD: Catalytic domain. LR: Linker region. CBM: Carbohydrate-binding module.

2.2. Cloning, Expression, and Purification of the AcCel12B and Its Mutants

The modular structure of AcCel12B and its mutants is shown in Figure 1. The three mutants were obtained by deleting or adding the PT/S-box unit. AcCel12B-PT0 and AcCel12B-PT1 were generated by deleting all or one PT/S-box unit from the wild type (AcCel12B-wt). The mutant AcCel12B-PT3 was generated by adding a PT/S-box unit, and all three PT/S-box units were axisymmetrically arranged and separated by a glycine. The mutants were generated by overlapping polymerase chain reaction (PCR) or whole-plasmid PCR using the primers listed in Table S1. The PCR fragments were inserted into the expression vector pET-20b and transformed into *Escherichia coli* BL21-Gold (DE3)-competent cells.

Expression of the wild-type and mutant AcCel12B was induced by isopropyl- β -D-1-thiogalactopyranoside (IPTG) in Luria Bertani (LB) medium [21]. Cells were harvested and disrupted by ultrasonic treatment. The recombinant proteins, AcCel12B-PT0, AcCel12B-PT1, AcCel12B-wt and AcCel12B-PT3, containing a C-terminal polyhistidine ($6 \times$ His) tag, were purified by affinity chromatography using Ni-NTA column. The homogeneity and purity of all proteins were analyzed by SDS/PAGE (Figure 2). The purity of cellulases was more than 95%. The apparent molecular weight (AM) of AcCel12B-wt and its mutants were determined by ImageJ (<http://rsb.info.nih.gov/ij/>) as indicated in Figure 1. The AM of the recombinant proteins were slightly different from the molecular weight (MW) calculated theoretically using ExPASy (http://web.expasy.org/compute_pi/). The AM of AcCel12B-PT3 and AcCel12B-wt were 5.6 and 2.7 kDa that higher than the expected MW, the AM and MW of AcCel12B-PT1 were identical, whereas the AM of AcCel12B-PT1 was 3.6 kDa lesser than MW. These results indicate

that the PT-box enabled protein with an extended dimension. Similar results have also been reported previously, wherein linker deletion changed protein topology, as analyzed by SAXS [11,30].

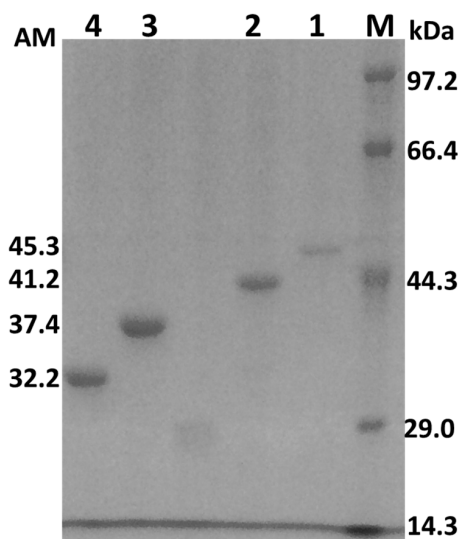


Figure 2. SDS-polyacrylamide gel electrophoresis of the wild-type and mutant AcCel12B. Lane M: Protein marker. Lane 1: AcCel12B-PT3. Lane 2: AcCel12B-wt. Lane 3: AcCel12B-PT1. Lane 4: AcCel12B-PT0. AM: Apparent molecular mass (kDa). SDS: Sodium dodecyl sulfate.

2.3. Enzymatic Activities

To assess the effects of the PT/S-box on enzymatic activities, the activity of AcCel12B and mutants towards various substrates was determined (Table 1). The thermal stability and optimum temperature and pH required for enzyme action did not vary significantly between wild-type and mutant AcCel12B (Figures S1 and S2). The optimal pH and temperature for enzyme activity of wild-type and mutant AcCel12B were 4.5 and 75 °C, respectively. The residual activities of AcCel12B and mutants were >96% at 60 °C for 5 h. The specific activities of the recombinants towards the soluble substrate, carboxymethyl cellulose (CMC), were similar except for that of AcCel12B-PT1, the activity of which was slightly lower than for the others. Although all the recombinants showed identical activity towards regenerated amorphous cellulose (RAC), the specific activity increased slightly but regularly with the number of PT/S-box units in the recombinants. The activities of the wild-type and mutant enzymes towards CMC and RAC were identical, and were much higher than those towards the crystalline substrate Avicel, which were similar to those reported previously [21]. Therefore, the number of PT/S-box units in the LR did not affect the substrate selection of AcCel12B. An obvious change was observed in the activity of the enzymes towards Avicel, which observably increased with the number of PT/S-box units. Accordingly, there was a regular increase in the specific activity (about 4.8 mU/μM) for Avicel as a function of PT/S-box unit. Other researchers have also reported that the deletion of the PT-box or LR affects enzyme activity. For example, deletion of the PT linker of the chimeric cellulase, EngD-PT-CBD, decreased endoglucanase activity (CMCase) by more than 3 folds [15]. Deletion of the linker peptide of cellobiohydrolase I from *Trichoderma reesei* decreased its degradation rate for crystalline cellulose [6]. The activities of endoglucanase A (CenA) from *Cellulomonas fimi* towards CMC, phosphoric acid-swollen cellulose (PASC), and Avicel deceased by two folds after deleting the PT/S-box [11]. In our case, the effect of the number of PT/S-box units on enzymatic activity towards various types of substrates was considerably different. Our results suggested that the PT/S-box of AcCel12B showed no obvious effect on activity towards soluble substrates, whereas it showed a weak effect on activity towards amorphous substrates and a strong effect on activity towards crystalline substrates. Furthermore, longer PT/S-boxes may be favorable for enzyme activity towards crystalline cellulose and less favorable for activity on amorphous cellulose.

Table 1. Enzyme activity against a range of cellulosic substrates.

Enzyme	Specific Activity		
	CMC * (U/μM)	RAC * (U/μM)	Avicel (mU/μM)
AcCel12B-PT0	2.8 ± 0.4	2.0 ± 0.1	8.3 ± 2.7
AcCel12B-PT1	2.2 ± 0.2	2.1 ± 0.2	12.0 ± 2.9
AcCel12B-wt	2.6 ± 0.3	2.4 ± 0.1	16.5 ± 1.1
AcCel12B-PT3	2.6 ± 0.3	2.7 ± 0.2	22.7 ± 3.4

* CMC: carboxymethyl cellulose. RAC: regenerated amorphous cellulose.

2.4. Time Course of Hydrolysis of AcCel12B and Its Mutants

As we previously indicated, the hydrolysis of insoluble substrates by wild-type AcCel12B is performed in multiple reaction steps that can be divided into an initial rapid phase and a later slow phase [21]. The insoluble substrates RAC and Avicel were used to determine the role of the PT/S-box in catalysis. However, the activity of wild-type and mutant AcCel12B on Avicel were not high enough to determine the initial rapid phase. Thus, RAC was the sole substrate used in this section. Enzyme catalysis was examined by incubating wild-type and mutant AcCel12B with RAC for various time durations and then measuring the amounts of reducing ends in the supernatant and pellet, respectively (Figure 3). The hydrolytic generation of reducing ends from the substrate by cellulases was previously reported to be best fitted by a power function described by Kostylev et al. [31], as mentioned below.

$$P_{\text{tot}} = At^b \quad (1)$$

where P_{tot} is the total generated product (reducing sugars in this case), b is the hydrolysis power factor, and A and t are the activity of the enzyme and the reaction time, respectively. As indicated in Figure 3A, the power function fitted well ($R^2 \geq 0.99$) to the generation of reducing sugars over time by wild-type and mutant AcCel12B. The fitted curves of wild-type and mutant AcCel12B showed a regular change with the number of PT/S-box units. The parameters A and b of wild-type and mutant AcCel12B in Equation (1) were calculated using the software OriginPro 8.0, as described by Kostylev et al. [31] (Table 2). The b values of wild-type and mutant AcCel12B showed no difference. The other cellulases, such as TfCel9A and TfCel48A from *Thermobifida fusca*, are modular enzymes, and the CBM of these two enzymes are associated with substrate binding efficiency [32,33]. However, when the CBM were deleted, the b value did not change, which suggested that the CBM did not directly assist the CD in substrate digestion [31]. Since the b values did not change with the number of PT/S-box units, we suggested that the PT/S-box of AcCel12B cannot change the intrinsic ability of the enzyme to overcome substrate recalcitrance. On the contrary, the A values of wild-type and mutant AcCel12B gradually increased in a step of 4 μM/min per PT/S-box unit added. This indicates that the PT/S-box of AcCel12B might affect the inherent specific activity or the amount of productively bound enzyme, as described by the two-parameter kinetic model [31]. Theoretically, the non-processive endoglucanases perform a repeated non-processive attack in the same region to produce soluble and insoluble ends. Hence, we speculated that the PT/S-box addition between CD and CBM might increase the enzyme attacking area on the cellulose surface, which increased the amount of productively bound enzyme. According to our previous study, the generation rate of soluble (SRE) and insoluble (IRE) ends during RAC hydrolysis by AcCel12B can be roughly divided into an initial rapid phase and a later slow phase. The rapid phase of IRE (RPI) and SRE (RPS) appear in the first 10 and 20 min time periods, respectively, which are followed by the slow phases of IRE (SPI) and SRE (SPS), respectively [21]. The duration of RPI or RPS will change correspondingly if PT/S-box addition or deletion increases or decreases the CD attacking area. However, the duration of RPI or RPS did not change with addition or deletion of PT/S-box unit (Figure 3B,C). Since the generation rate of the reducing ends of RPI or RPS increased linearly, we calculated the catalytic rate of individual phases using the linear fitting program of OriginPro 8.0 (Table 3). The results showed that the catalytic rate of wild-type and mutant

AcCel12B-wt in RPS and SPS were not significantly different. Therefore, the PT/S-box of AcCel12B did not affect the soluble end production. On the other contrary, the PT/S-box played an obvious function in IRE formation. The generation rates of RPI and SPI were reduced by approximately 0.41 and 0.33 folds, respectively, when the PT/S-box was completely deleted. Furthermore, the increase in the number of PT/S-box units increased the generation rate of RPI. Combined with the above results and discussion, we concluded that the PT/S-box affected the inherent specific activity of IRE production but not the amount of productively bound enzyme. This conclusion was partially confirmed by the result of the processivity assay (soluble/insoluble product ratio) of wild-type and mutant AcCel12B at each indicated incubation time point (Figure 3D). The processivity of wild-type and mutant AcCel12B increased linearly within the first 20 min of incubation, and then reached the maximum value either early or late, which showed that the processivity of wild-type and mutant AcCel12B was reduced with the number of PT/S-box units. Thus, longer PT/S-boxes between CD and CBM were favorable for IRE production by AcCel12B.

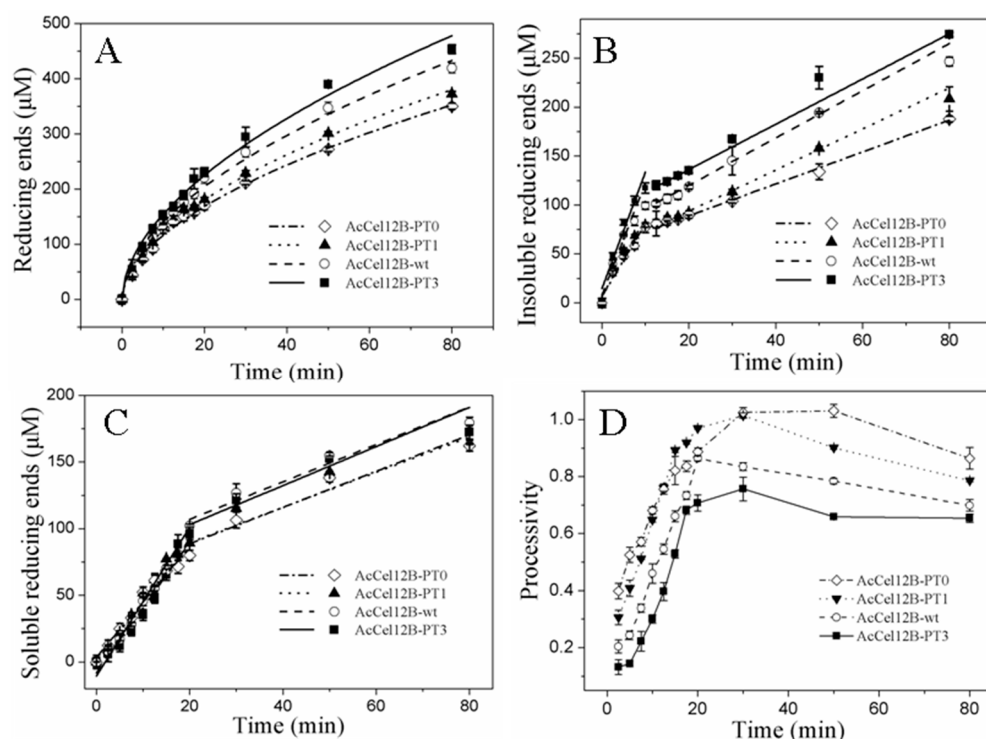


Figure 3. Time course of hydrolysis of RAC by wild-type AcCel12B and its mutants. (A) AcCel12B and its mutants were incubated with RAC and the reducing ends generated was calculated and fitted to Equation (1). (B,C) Time course of insoluble reducing ends (B) and soluble reducing ends (C) of the hydrolysis of RAC by AcCel12B and its mutants. (D) The processivity of AcCel12B and its mutants at indicated time points. RAC incubated with thermal inactivated recombinant protein was used as a blank. All data were averaged from triplicate measurements.

Table 2. Fitting curve parameters of the time course of RAC hydrolysis.

Enzyme	A ($\mu\text{M}/\text{min}$)	b ($\mu\text{M}/\text{min}$)	R ²
AcCel12B-PT0	33.7 ± 1.7	0.54 ± 0.01	0.995
AcCel12B-PT1	36.1 ± 1.8	0.54 ± 0.01	0.995
AcCel12B-wt	40.3 ± 2.6	0.54 ± 0.02	0.990
AcCel12B-PT3	44.1 ± 3.6	0.54 ± 0.02	0.990

Table 3. The rate distribution of reducing ends in time course of RAC hydrolysis.

Enzyme	Generation Rate of IRE *				Generation Rate of SRE *			
	RPI * ($\mu\text{M}/\text{min}$)	R^2	SPI * ($\mu\text{M}/\text{min}$)	R^2	RPS * ($\mu\text{M}/\text{min}$)	R^2	SPS * ($\mu\text{M}/\text{min}$)	R^2
AcCel12B-PT0	7.8 \pm 1.3	0.94	1.6 \pm 0.03	0.97	4.5 \pm 0.3	0.96	1.4 \pm 0.3	0.95
AcCel12B-PT1	10.8 \pm 1.4	0.94	2.1 \pm 0.06	0.99	4.8 \pm 0.1	0.99	1.3 \pm 0.2	0.85
AcCel12B-wt	13.3 \pm 1.2	0.91	2.4 \pm 0.1	0.98	4.8 \pm 0.2	0.99	1.5 \pm 0.2	0.96
AcCel12B-PT3	14.1 \pm 1.7	0.91	2.3 \pm 0.05	0.99	4.5 \pm 0.4	0.97	1.4 \pm 0.3	0.90

* IRE: Insoluble reducing ends. SRE: Soluble reducing ends. RPI: Rapid phase of insoluble reducing ends. RPS: Rapid phase of soluble reducing ends. SPI: Slow phase of insoluble reducing ends. SPS: Slow phase of soluble reducing ends.

2.5. Adsorption and Desorption of Wild-Type and Mutant AcCel12B

The adsorption and desorption properties of wild-type and mutant AcCel12B were obtained. The enzymes were incubated with Avicel and RAC individually, followed by desorption by increasing the concentration of sodium dodecyl sulfate (SDS) (Figure 4). The experimental data of adsorption was adjusted to the Langmuir isotherm equation. The E_{\max} (maximum adsorption capacities) of wild-type and mutant AcCel12B were not significantly different. Furthermore, the binding capacity of enzymes to RAC was 10 times higher than that to Avicel, which was similar to that reported by Hong et al. [34]. The E_{\max} of wild-type and mutant AcCel12B to Avicel and RAC were not different from those of other cellulases [34,35]. Srisodsuk et al. previously noted that the linker deletions of CBH I from *Trichoderma reesei* did not affect the enzyme affinity on crystalline cellulose at an initial enzyme concentration of 0.2 μM (5–9% saturation), but decreased the binding capacity as the enzyme concentration approached 10 μM [6]. Beckham et al. later explained this result by stating that the shortening of the tether between CD and CBM caused less enzyme extension [36]. In our case, the changes in PT/S-box number did not affect enzyme binding on the insoluble substrates irrespective of enzyme concentration. One possible explanation is that the PT/S-box of the wild-type AcCel12B was part of the full-length linker, and therefore, PT/S-box deletion or addition did not affect the enzyme extension and substrate affinity. Hence, we suggested that the activity difference between wild-type and mutant AcCel12B on Avicel and RAC were not due to differences in affinity.

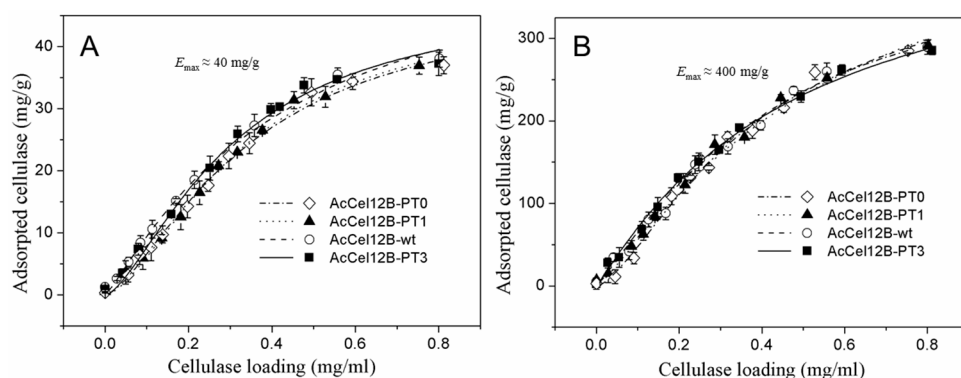


Figure 4. Adsorption of AcCel12B and its mutants on Avicel (A) and RAC (B). All the figures were described as AcCel12B-PT0 (dashed dotted line and \diamond), AcCel12B-PT1 (dotted line and \blacktriangle), AcCel12B-wt (dashed line and \circ), and AcCel12B-PT3 (solid line and \blacksquare).

The various methods used to study the desorption process included multiple washings with water [37], Tween solution, SDS solution [38,39], strong alkaline reagent [39], and nonionic surfactant [40]. In our study, the Avicel and RAC were adsorbed sufficiently by enzymes to be an equilibrium state. Then, they were firstly washed by low concentration of SDS (0.1% g/mL) to remove non-specific binding proteins. Then, the solid-bonded enzymes were desorbed by increasing the SDS concentration. The amount of desorbed protein was determined from the UV absorption values at

280 nm (Figure 5) and analyzed by SDS-polyacrylamide gel electrophoresis (SDS-PAGE) (Figures S3 and S4). The Freundlich (equilibrium) model is a commonly used approach for determining reagent distribution between solid and solution for both adsorption and desorption processes [41,42]. We used the Freundlich model to determine cellulase desorption. Experimental data of desorption was adjusted to the Freundlich equation and is expressed as

$$E = K_f \cdot C_S^n \quad (2)$$

where E and C_S are the equilibrium enzyme and SDS concentrations in the supernatant, respectively; K_f is the enzyme unit-capacity coefficient; n is a joint measure of the relative magnitude and diversity of energies of SDS and enzymes associated with a particular sorption process.

The solid-bonded protein was rapidly desorbed from Avicel and RAC in the low-concentration range of SDS, followed by gradual desorption at high concentrations of SDS (Figure 5). The amount of desorbing cellulases correlated linearly with low SDS concentrations (Figure 5A,B insertion). Therefore, the slopes of linear fit of desorption were obtained at low SDS concentration (Table 4). At the same SDS concentration, the amount of desorbed protein increased with the number of PT/S-box units. These results suggested that the wild-type and mutant AcCel12B enzymes containing more PT/S-box units were easily desorbed from cellulose in low SDS concentration ranges. The desorption of wild-type and mutant AcCel12B was also significantly different at high SDS concentrations (Figure 5). The parameters K_f and n of wild-type and mutant AcCel12B were calculated (Table 5). The K_f values of cellulases desorbing from Avicel reduced gradually in a step of approximately $0.6 \text{ (mg/g)/(g/mL)}^n$ per PT/S-box unit added. The K_f values of cellulases desorbing from RAC reduced unevenly with the number PT/S-box units. The decrease of AcCel12B-PT0 to AcCel12B-PT1 and AcCel12B-wt to AcCel12B-PT3 was approximately $7.0 \text{ (mg/g)/(g/mL)}^n$. The decrease of AcCel12B-PT1 to AcCel12B-wt was approximately $1.0 \text{ (mg/g)/(g/mL)}^n$. The date of K_f illustrated the amount of cellulases that adsorbed on the cellulose. Studies show that K_f was related to the molecular size and adsorbate-solvent interactions [43]. SDS-PAGE showed that the molecular size of cellulases increased with the number of PT/S-box units of the recombinants (Figure 2). Previously, studies using SAXS demonstrated that linker deletion altered protein topology [11,30]. Hence, the differences in the size of the protein molecules may explain the diverse K_f values of wild-type and mutant AcCel12B.

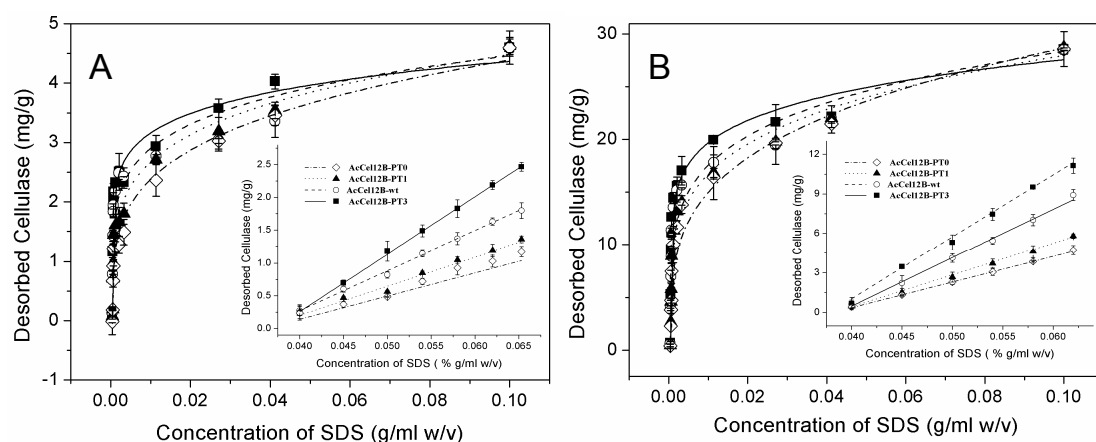


Figure 5. Desorption of AcCel12B and its mutants from Avicel and RAC. (A) Desorption of cellulases from Avicel. (B) Desorption of cellulases from RAC. The concentration of desorbed proteins was measured by A280nm, calculated, and fitted in Equation (2). The amount of cellulases desorbing from cellulose under low SDS conditions was linearly fitted. All figures were described as AcCel12B-PT0 (dashed dotted line and \diamond), AcCel12B-PT1 (dotted line and \blacktriangle), AcCel12B-wt (dashed line and \circ), and AcCel12B-PT3 (solid line and \blacksquare).

Table 4. Linear fitting curve parameters of desorption of AcCel12B and its mutants at low SDS concentrations (0.04–0.065% g/mL).

Enzyme	Avicel		RAC	
	Slope	R ²	Slope	R ²
AcCel12B-PT0	35.5 ± 2.5	0.88	193.6 ± 4.8	0.99
AcCel12B-PT1	44.4 ± 2.2	0.94	240.7 ± 9	0.99
AcCel12B-wt	61.1 ± 3.1	0.99	367.4 ± 20	0.99
AcCel12B-PT3	87.6 ± 3.1	0.99	470.2 ± 12	0.99

Table 5. Fitting curve parameters for desorption of AcCel12B and its mutants.

Enzyme	Avicel			RAC		
	K _f (mg/g)/(g/mL) ⁿ	n	R ²	K _f (mg/g)/(g/mL) ⁿ	n	R ²
AcCel12B-PT0	8.0 ± 0.5	0.26 ± 0.02	0.99	54.4 ± 3.2	0.28 ± 0.02	0.98
AcCel12B-PT1	7.4 ± 0.9	0.22 ± 0.02	0.95	46.5 ± 2.4	0.22 ± 0.02	0.99
AcCel12B-wt	6.8 ± 1.0	0.18 ± 0.02	0.87	45.4 ± 3.3	0.20 ± 0.02	0.97
AcCel12B-PT3	6.0 ± 0.6	0.14 ± 0.02	0.92	38.5 ± 3.9	0.14 ± 0.02	0.94

Furthermore, n in Table 5 indicates sorption intensity [44], or the energy of desorption [42]. The n values of wild-type and mutant AcCel12B desorbing from Avicel reduced gradually with the number PT/S-box units in a step of approximately 0.4 per PT/S-box unit added. The n values of cellulases desorbing from RAC were unevenly reduced with the number of PT-box units. The decrease of AcCel12B-PT0 to AcCel12B-PT1 and AcCel12B-wt to AcCel12B-PT3 was approximately 0.6. The decrease of AcCel12B-PT1 to AcCel12B-wt was approximately 0.2. This unevenness may be caused by the irregularity of RAC-specific surface. These results illustrated that the energy of AcCel12B mutants desorbing from cellulose decreased with the number of PT-box units, and AcCel12B containing more PT/S-box units were easily desorbed from cellulose. These results combined with those of wild-type and mutant AcCel12B containing longer PT-boxes showed a higher specific activity for Avicel and RAC (Table 1). We thus suggested that desorption of AcCel12B from cellulose might play a key role in catalysis. The easily desorbed AcCel12B had more opportunity for hydrolyzing cellulose. Studies showed that the planar binding surface of the CBM that contained three tyrosine residues adhered to the hydrophobic face of cellulose comprising the axial H1, H3, and H5 aliphatic protons [45,46]. Liu et al. observed that cellobiohydrolase-only hydrolyzed crystalline cellulose on the hydrophobic (110) faces of microcrystalline cellulose [47]. The hydroxyl groups of sugar chains were arranged outwardly in a regular order in the 110 surface of microcrystalline cellulose [25]. Shen et al. reported that deletion of the PT/S-box in the linker changed the desorption process of cellulose [11].

Our study proposes a PT/S-box unit of AcCel12B and clearly confirms that the number of PT/S-box units in endocellulases affects the desorption of the enzyme and that the differences in the activity of wild-type and mutant AcCel12B on Avicel and RAC is due to differences in desorption. We thus suggest that there may be an interaction between insoluble cellulose and T or S of PT/S-box, and that the interaction is favorable for the desorption of AcCel12B. Further direct evidence is needed to reveal the interactions between the PT/S-box and cellulose. This will be helpful for the design of modular endocellulases.

3. Materials and Methods

3.1. Strains, Vectors, and Materials

For cloning and expression of the wild-type and mutant genes (ABK52392), *E. coli* DH5 α (Invitrogen, Carlsbad, CA, USA) and *E. coli* BL21-Gold (DE3) (Novagen, Madison, WI, USA) were used

as hosts for propagation and overexpression, respectively. The plasmid pET-20b (Novagen) was used as an expression vector. The recombinant plasmid pET20b-AcCel12B described by Wang et al. [21] was used as the template for constructing the mutants. Genomic DNA purification kit was obtained from AxyPrep (AxyPrep, Shanghai, China). Restriction endonucleases, LA Taq DNA polymerase, and DNA purification kit were obtained from TaKaRa (TaKaRa Bio, Dalian, China). T4 DNA ligase and Dpn I were purchased from New England Biolabs (Beverley, MA, USA). CMC (low viscosity) and Avicel® PH101 (50 μm particle size) were purchased from Sigma-Aldrich (St. Louis, MO, USA). Regenerated amorphous cellulose (RAC) was prepared from Avicel® PH101 as described by Zhang [48]. All other chemicals were of analytical grade.

3.2. Construction of Mutant Plasmids

For construction of mutant AcCel12B-PT0, the pET20b-AcCel12B plasmid was used as the template and primer pairs 1–3 and 2–4 were used to generate the sequences encoding CD and CBM, respectively. Overlap PCR was performed using the CD and CBM-encoding sequences and the primer pairs 1–4. The PCR product was isolated and ligated into the vector pET-20b as described by Wang et al. [21]. The whole-plasmid PCR cloning method was performed for obtaining the mutants AcCel12B-PT1 and the AcCel12B-PT3. The plasmid pAcCel12B-PT1 was obtained by primers 5 and 6 using plasmid pAcCel12B-PT0 as the template. The plasmid pAcCel12B-PT3 was obtained using primers 7 and 8 and the plasmid pET20b-AcCel12B as a template. All the primers used in the construction are listed in Supplementary Materials: Table S1. The whole-plasmid PCR conditions consisted of an initial step (94°C for 4 min), followed by 30 cycles of 94°C for 10 s, 55°C for 30 s and 72°C for 5 min, and a final elongation step (72°C for 5 min). All the plasmids were transformed into *E. coli* DH5 α and sequenced to confirm the fidelity of the constructs. The plasmids were then isolated and transformed into *E. coli* BL21-Gold (DE3) for recombinant expression.

3.3. Expression and Purification of Wild-Type and Mutant AcCel12B

The wild-type and mutant AcCel12B were expressed in *E. coli* BL21-Gold (DE3). Cells were grown to an OD₆₀₀ of 0.6 in LB medium containing $50 \mu\text{g}\cdot\text{mL}^{-1}$ ampicillin at 37°C . Protein expression was induced by adding 1 mM isopropyl- β -D-1-thiogalactopyranoside (IPTG), with an inducing temperature and time of 15°C and 20 h, respectively. The cells were harvested and resuspended in buffer A (50 mM sodium phosphate, pH 7.0) and then disrupted by ultrasonic treatment at 4°C . The cell debris was removed by centrifugation at 12,000 rpm for 20 min. The supernatant of the crude extract was loaded onto a Ni-NTA column (Qiagen, Valencia, CA, USA) that had been equilibrated with buffer A and eluted using linear concentrations imidazole. The eluted protein was dialyzed with buffer A and analyzed by 12% SDS-PAGE stained with Coomassie Blue. Protein concentrations were measured using Bradford assay [49] with bovine serum albumin as the standard.

3.4. Enzyme Activity Assay

The endoglucanase activities of wild-type and mutant AcCel12B were determined by incubating the enzymes with CMC (1%, *w/v*) and RAC (0.5%, *w/v*) at 60°C for 5 and 10 min, and with Avicel (1%, *w/v*) at 60°C for 3 h, respectively. Sodium acetate buffer (50 mM, pH 4.5) was used for all assay steps unless otherwise described. The concentration of reducing ends was determined by the 3,5-dinitrosalicylic acid (DNS) method using glucose as a standard, as previously described [50]. The absorbance at 540 nm was measured using a UV-2550 spectrophotometer (Shimadzu, Kyoto, Japan). One unit (U) of cellulase activity was defined as the amount of enzyme catalyzing the release of 1 μmol of reducing sugar per min.

3.5. Enzyme Characterization

To determine the activities of wild-type and mutant AcCel12B at different pH values, reactions were performed at 70°C in indicated buffer. The effect of temperature on wild-type and mutant

AcCel12B was determined in 50 mM sodium acetate buffer (pH 4.5) by incubating reaction mixtures at different temperatures ranging from 40 to 90 °C. For measurement of thermostability, the wild-type and mutant AcCel12B were incubated at 60 °C for various durations. The residual activity of enzyme was then determined by incubating the enzyme with CMC (1%, *w/v*) for 5 min.

3.6. Time Course of Hydrolysis

One hundred microliters of reaction mixtures containing 0.2 μM enzymes and 0.5% (*w/v*) RAC were performed in 2 mL Eppendorf centrifuge tubes on a heating block at 70 °C with mixing (900 rpm). At the required time points, the tubes were removed and placed in salt-ice mixture to stop the reaction. The insoluble RAC was separated by centrifugation (5 min, 12,000×*g*). The pellet was washed thrice with sodium acetate buffer and separated by centrifugation at 4 °C. The concentration of reducing ends in the collected supernatant and pellet was determined by DNS method. Samples containing thermal denatured enzyme were used as a blank. All experiments were performed in triplicate.

3.7. Enzyme Adsorption and Desorption Assays

AvicelPH101 and RAC were used to determine the adsorption of cellulase on insoluble substrates. Adsorption was performed at 4 °C in 2 mL Eppendorf centrifuge tubes. Two hundred microliter mixtures containing 5.0 mg Avicel or 0.6 mg RAC and 0–0.8 mg of protein in sodium acetate buffer (50 mM, pH 4.5) were incubated at 4 °C for 60 min with mixing (900 rpm), followed by centrifugation at 12,000 rpm for 5 min at 4 °C. The concentrations of unbound protein were determined according to UV absorption at 280 nm, as described by Reinikainen [51]. The amount of adsorbed proteins was estimated from the difference between the initial protein concentration and the unbound protein concentration.

Mixtures containing 0.8 mg enzymes and Avicel (5.0 mg) or RAC (0.5 mg) in 200 μL sodium acetate buffer (50 mM, pH 4.5) were incubated at 4 °C for 60 min with mixing (900 rpm). Then the mixtures were centrifuged at 12,000 rpm for 5 min at 4 °C. Avicel and RAC were sufficiently adsorbed by wild-type and mutant AcCel12B of equal mass to be in an equilibrium state that was washed repeatedly at low SDS concentration (0.01% g/mL) until the supernatant had no UV absorption at 280 nm. Then, the Avicel or RAC bound to the proteins in equilibrium were incubated with various concentrations of SDS (200 μL) at 4 °C for 5 min upon mixing (900 rpm) and then centrifuged at 12,000 rpm for 5 min. The identity and concentrations of desorbed protein in the supernatant were determined by SDS-PAGE and UV absorption at 280 nm, respectively, as indicated above.

4. Conclusions

We cloned, expressed, and purified wild-type AcCel12B and three mutants with different linker lengths and observed that the activity of cellulases on insoluble cellulose increased with the number PT/S-box units; however, no significant difference in activity was observed with soluble cellulose. The hydrolysis course of RAC was accelerated with the number of PT/S-box units of AcCel12B. AcCel12B containing different numbers of PT/S-box units had similar processivity. The desorption processes of wild-type and mutant AcCel12B from RAC and Avicel were significantly different. The energy of desorption of wild-type and mutant AcCel12B from cellulose decreased with the number of PT/S-box units. AcCel12B with more PT/S-box units was easily desorbed from cellulose and had more opportunity to hydrolyze cellulose. Thus, the number of PT/S-box units in endocellulases affected the desorption process of the enzyme, and the activity difference between wild-type and mutant AcCel12B on Avicel and RAC is due to differences in desorption.

Supplementary Materials: The following are available online at <http://www.mdpi.com/2073-4344/8/3/123/s1>, Table S1: Oligonucleotides used as primers in PCR, Figure S1: Effects of pH and temperature on activity of AcCel12B-wt (■) and mutant AcCel12B-PT0 (○) toward substrate CMC and substrate RAC, Figure S2: Thermal stability of AcCel12B and its mutants in at 60 °C, Figure S3: SDS-Polyacrylamide gel electrophoresis of AcCel12B-PT3 and AcCel12B-wt desorbing from RAC, Figure S4: SDS-Polyacrylamide gel electrophoresis of AcCel12B-PT0 and AcCel12B-PT1 desorbing from Avicel.

Acknowledgments: This work is supported by the “973” program of China (2012CB721003), Sic-Tech Development of Jilin Province (20170204040GX), and Department of Education of Jilin Province (2016-438). We sincerely thank Chunyu Wang (State Key Laboratory of Supramolecular Structure and Materials, College of Chemistry, Jilin University, China) for technical assistance.

Author Contributions: Z.Z. and Y.L. conceived and designed the experiments; Y.L., J.W., L.W., H.T., M.B. and G.G. performed the experiments; Y.L., W.H. and Z.Z. analyzed the data; Z.Z. and Y.L. wrote the paper.

Conflicts of Interest: The authors declare no conflict of interest.

References

1. Béguin, P.; Aubert, J.P. The biological degradation of cellulose. *FEMS Microbiol. Rev.* **1994**, *13*, 25–58. [[CrossRef](#)] [[PubMed](#)]
2. Wood, T.M.; McCrae, S.I.; Bhat, K.M. The mechanism of fungal cellulase action. Synergism between enzyme components of *Penicillium pinophilum* cellulase in solubilizing hydrogen bond-ordered cellulose. *Biochem. J.* **1989**, *260*, 37–43. [[CrossRef](#)] [[PubMed](#)]
3. Beguin, P. Molecular Biology of Cellulose Degradation. *Annu. Rev. Microbiol.* **1990**, *44*, 219–248. [[CrossRef](#)] [[PubMed](#)]
4. Sonan, G.K.; Receveur-Brechot, V.; Duez, C.; Aghajari, N.; Czjzek, M.; Haser, R.; Gerday, C. The linker region plays a key role in the adaptation to cold of the cellulase from an Antarctic bacterium. *Biochem. J.* **2007**, *407*, 293–302. [[CrossRef](#)] [[PubMed](#)]
5. Zhang, Y.-H.P.; Lynd, L.R. Toward an aggregated understanding of enzymatic hydrolysis of cellulose: Noncomplexed cellulase systems. *Biotechnol. Bioeng.* **2004**, *88*, 797–824.
6. Srisodsuk, M.; Reinikainen, T.; Penttilä, M.; Teeri, T.T. Role of the interdomain linker peptide of *Trichoderma reesei* cellobiohydrolase I in its interaction with crystalline cellulose. *J. Biol. Chem.* **1993**, *268*, 20756–20761. [[PubMed](#)]
7. Strobel, K.L.; Pfeiffer, K.A.; Blanch, H.W.; Clark, D.S. Engineering Cel7A carbohydrate binding module and linker for reduced lignin inhibition. *Biotechnol. Bioeng.* **2016**, *113*, 1369–1374. [[CrossRef](#)] [[PubMed](#)]
8. Kont, R.; Kari, J.; Borch, K.; Westh, P.; Välijamäe, P. Inter-domain Synergism Is Required for Efficient Feeding of Cellulose Chain into Active Site of Cellobiohydrolase Cel7A. *J. Biol. Chem.* **2016**, *291*, 26013–26023. [[CrossRef](#)] [[PubMed](#)]
9. Sammond, D.W.; Payne, C.M.; Brunecky, R.; Himmel, M.E.; Crowley, M.F.; Beckham, G.T. Cellulase linkers are optimized based on domain type and function: Insights from sequence analysis, biophysical measurements, and molecular simulation. *PLoS ONE* **2012**, *7*, e48615. [[CrossRef](#)] [[PubMed](#)]
10. Raymond-Wong, W.K.; Gerhard, B.; Guo, Z.M.; Kilburn, D.G.; Anthony, R.; Warren, J.; Miller, R.C. Characterization and structure of an endoglucanase gene cenA of *Cellulomonas fimi*. *Gene* **1986**, *44*, 315–324. [[CrossRef](#)]
11. Shen, H.; Schmuck, M.; Pilz, I.; Gilkes, N.R.; Kilburn, D.G.; Miller, R.C.; Warren, R.A. Deletion of the linker connecting the catalytic and cellulose-binding domains of endoglucanase A (CenA) of *Cellulomonas fimi* alters its conformation and catalytic activity. *J. Biol. Chem.* **1991**, *266*, 11335–11340. [[PubMed](#)]
12. Poon, D.K.; Withers, S.G.; McIntosh, L.P. Direct demonstration of the flexibility of the glycosylated proline-threonine linker in the *Cellulomonas fimi* Xylanase Cex through NMR spectroscopic analysis. *J. Biol. Chem.* **2007**, *282*, 2091–2100. [[CrossRef](#)] [[PubMed](#)]
13. Sunna, A.; Gibbs, M.D.; Chin, C.W.; Nelson, P.J.; Bergquist, P.L. A gene encoding a novel multidomain beta-1,4-mannanase from *Caldibacillus cellulovorans* and action of the recombinant enzyme on kraft pulp. *Appl. Environ. Microbiol.* **2000**, *66*, 664–670. [[CrossRef](#)] [[PubMed](#)]
14. McCarter, S.L.; Adney, W.S.; Vinzant, T.B.; Jennings, E.; Eddy, F.P.; Decker, S.R.; Baker, J.O.; Sakon, J.; Himmel, M.E. Exploration of cellulose surface-binding properties of *acidothermus cellulolyticus* Cel5A by site-specific mutagenesis. *Appl. Biochem. Biotechnol.* **2002**, *98–100*, 273–287. [[CrossRef](#)]
15. Yeh, M.; Craig, S.; Lum, M.G.; Foong, F.C. Effects of the PT region of EngD and HLD of CbpA on solubility, catalytic activity and purification characteristics of EngD-CBD(CbpA) fusions from *Clostridium cellulovorans*. *J. Biotechnol.* **2005**, *116*, 233–244. [[CrossRef](#)] [[PubMed](#)]

16. Boze, H.; Marlin, T.; Durand, D.; Pérez, J.; Vernhet, A.; Canon, F.; Sarni-Manchado, P.; Cheynier, V.; Cabane, B. Proline-Rich Salivary Proteins Have Extended Conformations. *Biophys. J.* **2010**, *99*, 656–665. [[CrossRef](#)] [[PubMed](#)]
17. Receveur, V.; Czjzek, M.; Schülein, M.; Panine, P.; Henrissat, B. Dimension, shape, and conformational flexibility of a two domain fungal cellulase in solution probed by small angle X-ray scattering. *J. Biol. Chem.* **2002**, *277*, 40887–40892. [[CrossRef](#)] [[PubMed](#)]
18. Harrison, M.J.; Nouwens, A.S.; Jardine, D.R.; Zachara, N.E.; Gooley, A.A.; Nevalainen, H.; Packer, N.H. Modified glycosylation of cellobiohydrolase I from a high cellulase-producing mutant strain of *Trichoderma reesei*. *Eur. J. Biochem.* **1998**, *256*, 119–127. [[CrossRef](#)] [[PubMed](#)]
19. Ossowski, I.V.; Eaton, J.T.; Czjzek, M.; Perkins, S.J.; Frandsen, T.P.; Schülein, M.; Panine, P.; Henrissat, B.; Receveurbréchot, V. Protein Disorder: Conformational Distribution of the Flexible Linker in a Chimeric Double Cellulase. *Biophys. J.* **2005**, *88*, 2823–2832. [[CrossRef](#)] [[PubMed](#)]
20. Payne, C.M.; Resch, M.G.; Chen, L.; Crowley, M.F.; Himmel, M.E.; Nd, T.L.; Sandgren, M.; Ståhlberg, J.; Stals, I.; Tan, Z. Glycosylated linkers in multimodular lignocellulose-degrading enzymes dynamically bind to cellulose. *Proc. Natl. Acad. Sci. USA* **2013**, *110*, 14646–14651. [[CrossRef](#)] [[PubMed](#)]
21. Wang, J.; Gao, G.; Li, Y.; Yang, L.; Liang, Y.; Jin, H.; Han, W.; Feng, Y.; Zhang, Z. Cloning, Expression, and Characterization of a Thermophilic Endoglucanase, AcCel12B from Acidothermus cellulolyticus 11B. *Int. J. Mol. Sci.* **2015**, *16*, 25080–25095. [[CrossRef](#)] [[PubMed](#)]
22. Hurley, J.H.; Mason, D.A.; Matthews, B.W. Flexible-geometry conformational energy maps for the amino acid residue preceding a proline. *Biopolymers* **1992**, *32*, 1443–1446. [[CrossRef](#)] [[PubMed](#)]
23. Morgan, A.A.; Rubenstein, E. Proline: The distribution, frequency, positioning, and common functional roles of proline and polyproline sequences in the human proteome. *PLoS ONE* **2013**, *8*, e53785. [[CrossRef](#)] [[PubMed](#)]
24. Williamson, M.P. The structure and function of proline-rich regions in proteins. *Biochem. J.* **1994**, *297*, 249–260. [[CrossRef](#)] [[PubMed](#)]
25. Lahiji, R.R.; Xu, X.; Reifenberger, R.; Raman, A.; Rudie, A.; Moon, R.J. Atomic force microscopy characterization of cellulose nanocrystals. *Langmuir* **2010**, *26*, 4480–4488. [[CrossRef](#)] [[PubMed](#)]
26. Zimm, B.H.; Bragg, J.K. Theory of the Phase Transition between Helix and Random Coil in Polypeptide Chains. *J. Chem. Phys.* **1959**, *31*, 526–535. [[CrossRef](#)]
27. Ohkubo, Y.Z.; Brooks, C.L. Exploring Flory’s Isolated-Pair Hypothesis: Statistical Mechanics of Helix-Coil Transitions in Polyalanine and the C-Peptide from RNase A. *Proc. Natl. Acad. Sci. USA* **2003**, *100*, 13916–13921. [[CrossRef](#)] [[PubMed](#)]
28. Batista, P.R.; Costa, M.G.; Pascutti, P.G.; Bisch, P.M.; de-Souza, W. High temperatures enhance cooperative motions between CBM and catalytic domains of a thermostable cellulase: Mechanism insights from essential dynamics. *Phys. Chem. Chem. Phys.* **2011**, *13*, 13709–13720. [[CrossRef](#)] [[PubMed](#)]
29. Ting, C.L.; Makarov, D.E.; Wang, Z.G. A kinetic model for the enzymatic action of cellulase. *J. Phys. Chem. B* **2009**, *113*, 4970–4977. [[CrossRef](#)] [[PubMed](#)]
30. Abuja, P.M.; Schmuck, M.; Pilz, I.; Tomme, P.; ClaeysSENS, M.; Esterbauer, H. Structural and functional domains of cellobiohydrolase I from *Trichoderma reesei*. *Eur. Biophys. J.* **1988**, *15*, 339–342. [[CrossRef](#)]
31. Kostylev, M.; Wilson, D. Two-parameter kinetic model based on a time-dependent activity coefficient accurately describes enzymatic cellulose digestion. *Biochemistry* **2013**, *52*, 5656–5664. [[CrossRef](#)] [[PubMed](#)]
32. Irwin, D.C.; Zhang, S.; Wilson, D.B. Cloning, expression and characterization of a family 48 exocellulase, Cel48A, from *Thermobifida fusca*. *Eur. J. Biochem.* **2000**, *267*, 4988–4997. [[CrossRef](#)] [[PubMed](#)]
33. Irwin, D.; Shin, D.H.; Zhang, S.; Barr, B.K.; Sakon, J.; Karplus, P.A.; Wilson, D.B. Roles of the catalytic domain and two cellulose binding domains of *Thermomonospora fusca* E4 in cellulose hydrolysis. *J. Bacteriol.* **1998**, *180*, 1709–1714. [[PubMed](#)]
34. Hong, J.; Ye, X.; Wang, Y.; Zhang, Y.H.P. Bioseparation of recombinant cellulose-binding module-proteins by affinity adsorption on an ultra-high-capacity cellulosic adsorbent. *Anal. Chim. Acta* **2008**, *621*, 193–199. [[CrossRef](#)] [[PubMed](#)]
35. Machado, D.L.; Moreira-Neto, J.; da-Cruz, J.G.; Bonomi, A.; Rabelo, S.C.; da-Costa, A.C. Adsorption characteristics of cellulase and β -glucosidase on Avicel, pretreated sugarcane bagasse, and lignin. *Biotechnol. Appl. Biochem.* **2015**, *62*, 681–689. [[CrossRef](#)] [[PubMed](#)]

36. Beckham, G.T.; Bomble, Y.J.; Matthews, J.F.; Taylor, C.B.; Resch, M.G.; Yarbrough, J.M.; Decker, S.R.; Bu, L.; Zhao, X.; McCabe, C. The O-glycosylated linker from the *Trichoderma reesei* Family 7 cellulase is a flexible, disordered protein. *Biophys. J.* **2010**, *99*, 3773–3781. [[CrossRef](#)] [[PubMed](#)]
37. Ghose, T.K.; Bisaria, V.S. Studies on the mechanism of enzymatic hydrolysis of cellulosic substances. *Biotechnol. Bioeng.* **1979**, *21*, 131–146. [[CrossRef](#)] [[PubMed](#)]
38. Castanon, M.; Wilke, C.R. Adsorption and recovery of cellulases during hydrolysis of newspaper. *Biotechnol. Bioeng.* **1980**, *22*, 1037–1053. [[CrossRef](#)]
39. Otter, D.E.; Munro, P.A.; Scott, G.K. Desorption of *Trichoderma reesei* cellulase from cellulose by a range of desorbents. *Biotechnol. Bioeng.* **1989**, *34*, 291–298. [[CrossRef](#)] [[PubMed](#)]
40. Reese, E.T. Elution of Cellulase from Cellulose. *Process Biochem.* **1982**, *17*, 2.
41. Sankararamakrishnan, R.; Vishveshwara, S. Characterization of proline-containing α -helix (helix F model of bacteriorhodopsin) by molecular dynamics studies. *Proteins Struct. Funct. Inform.* **1993**, *15*, 26–41. [[CrossRef](#)] [[PubMed](#)]
42. Weber, W.J.; Young, T.M. A Distributed Reactivity Model for Sorption by Soils and Sediments. 6. Mechanistic Implications of Desorption under Supercritical Fluid Conditions. *Environ. Sci. Technol.* **1997**, *31*, 1686–1691. [[CrossRef](#)]
43. Furuya, E.G.; Chang, H.T.; Miura, Y.; Noll, K.E. A fundamental analysis of the isotherm for the adsorption of phenolic compounds on activated carbon. *Sep. Purif. Technol.* **1997**, *11*, 69–78. [[CrossRef](#)]
44. Núñez-Delgado, A.; Fernández-Sanjurjo, M.J.; Álvarez-Rodríguez, E.; Cutillas-Barreiro, L.; Nóvoa-Muñoz, J.; Arias-Estévez, M. Cr(VI) Sorption/Desorption on Pine Sawdust and Oak Wood Ash. *Int. J. Environ. Res. Public Health* **2015**, *12*, 8849–8860. [[CrossRef](#)] [[PubMed](#)]
45. Tavagnacco, L.; Mason, P.E.; Schnupf, U.; Pitici, F.; Zhong, L.; Himmel, M.E.; Crowley, M.; Cesàro, A.; Brady, J.W. Sugar-binding sites on the surface of the carbohydrate-binding module of CBH I from *Trichoderma reesei*. *Carbohydr. Res.* **2011**, *346*, 839–846. [[CrossRef](#)] [[PubMed](#)]
46. Taylor, C.B.; Talib, M.F.; McCabe, C.; Bu, L.; Adney, W.S.; Himmel, M.E.; Crowley, M.F.; Beckham, G.T. Computational Investigation of Glycosylation Effects on a Family 1 Carbohydrate-binding Module. *J. Biol. Chem.* **2012**, *287*, 3147–3155. [[CrossRef](#)] [[PubMed](#)]
47. Liu, Y.S.; Baker, J.O.; Zeng, Y.; Himmel, M.E.; Haas, T.; Ding, S.Y. Cellobiohydrolase Hydrolyzes Crystalline Cellulose on Hydrophobic Faces. *J. Biol. Chem.* **2011**, *286*, 11195–11201. [[CrossRef](#)] [[PubMed](#)]
48. Zhang, Y.H.P.; Cui, J.; Lynd, L.R.; Kuang, L.R. A transition from cellulose swelling to cellulose dissolution by o-phosphoric acid: Evidence from enzymatic hydrolysis and supramolecular structure. *Biomacromolecules* **2006**, *7*, 644–648. [[CrossRef](#)] [[PubMed](#)]
49. Bradford, M.M. A rapid and sensitive method for the quantitation of microgram quantities of protein utilizing the principle of protein-dye binding. *Anal. Biochem.* **1976**, *72*, 248–254. [[CrossRef](#)]
50. Ghose, T.K. Measurement of cellulase activities. *Pure Appl. Chem.* **1987**, *59*, 257–268. [[CrossRef](#)]
51. Reinikainen, T.; Teleman, O.; Teeri, T.T. Effects of pH and high ionic strength on the adsorption and activity of native and mutated cellobiohydrolase I from *Trichoderma reesei*. *Proteins* **1995**, *22*, 392–403. [[CrossRef](#)] [[PubMed](#)]



© 2018 by the authors. Licensee MDPI, Basel, Switzerland. This article is an open access article distributed under the terms and conditions of the Creative Commons Attribution (CC BY) license (<http://creativecommons.org/licenses/by/4.0/>).